Electrically Switchable, Polarization-Sensitive Encryption Based on Aluminum Nanoaperture Arrays Integrated with Polymer-Dispersed Liquid Crystals

Ke Li, Jiawei Wang, Wenfeng Cai, Huilin He, Mengjia Cen, Jianxun Liu, Dan Luo, Quanquan Mu, Davy Gérard, Yan Jun Liu

Electrically Switchable, Polarization-Sensitive Encryption Based on Aluminum Nanoaperture Arrays Integrated with Polymer-Dispersed Liquid Crystals

Ke Li[1,2], Jiawei Wang[1], Wenfeng Cai[1], Huilin He[1,3], Mengjia Cen[1], Jianxun Liu[1], Dan Luo[1], Quanquan Mu[4], Davy Gérard[2*], and Yan Jun Liu[1,4,5*]

[1]*Department of Electrical and Electronic Engineering, Southern University of Science and Technology, Shenzhen 518055, China*

[2]*Light, nanomaterials, nanotechnologies (L2n), Université de Technologie de Troyes & CNRS ERL 7004, 10004 Troyes, France*

[3]*Harbin Institute of Technology, Harbin 150001, China*

[4]*State Key Laboratory of Applied Optics, Changchun Institute of Optics, Fine Mechanics and Physics, Chinese Academy of Sciences, Changchun 130033, China*

[5]*Key Laboratory of Energy Conversion and Storage Technologies (Southern University of Science and Technology), Ministry of Education, Shenzhen 518055, China*

**Corresponding author*: davy.gerard@utt.fr; yjliu@sustech.edu.cn

KEYWORDS: Structural coloration, polarized encryption, nanoaperture array, polymer-dispersed liquid crystal, surface plasmon

ABSTRACT: Metasurface-based structural coloration is a promising enabling technology for advanced optical encryption with a high-security level. Herein, we propose a paradigm of electrically switchable, polarization-sensitive optical encryption based on designed metasurfaces

integrated with polymer-dispersed liquid crystals. The metasurfaces consist of anisotropic and isotropic aluminum nanoaperture arrays. Optical images can be encrypted by elaborately arranging anisotropic and isotropic nanoapertures based on their polarization-dependent plasmonic resonance characteristics. We demonstrate high-quality encrypted images and QR codes with electrically switchable, polarization-sensitive properties based on PDLC-integrated aluminum nanoaperture arrays. The proposed technique can be applied to many fields including high-security optical encryption, security tags, anti-counterfeiting, multichannel imaging, and dynamic displays.

Driven by the huge profits in the imitative commodities market, counterfeit goods have become an increasingly serious problem in society. Attaching security tags (identification labels) to goods that are hard to copy is a prevailing solution. Along this line, advanced optical encryption and identification techniques, such as metasurface-based holographic images and structural colorations, have been extensively studied to overcome the limitations of traditional anti-counterfeiting approaches.[1–3] Metasurfaces provide an unprecedented platform to manipulate the light field either spatially or temporally, including amplitude, phase, polarization, wavelength, etc.[4–7] Metasurface-enabled structural coloration, originating from light interaction with nanostructures, can revive the minutia with high accuracy.[8–11] However, this technique is often limited to a static single channel, which is controlled by the opto-geometrical parameters of both the meta-atoms and the surrounding media. Some efforts have been made to overcome this limit including polarization-sensitive nanostructures,[12–19] and stimuli-responsive composite systems.[20–28] These reported works always manifest complementary dual-images or embedded information

in another form.[15,19,20,24] Anisotropic nanostructures play a key role in realizing the above-mentioned functions. However, anisotropic nanoapertures and nanoantennas usually produce significant differences in coloration. For instance, a square arrangement of anisotropic metallic nanoantennas produces two colors, corresponding to nanoantennas' transverse and longitudinal modes. On the other hand, the same arrangement of anisotropic metallic nanoapertures with an optimized aspect ratio gives rise to a polarization-identifiable plasmonic resonance in the visible spectrum, resulting in a distinct coloration in one direction, but indiscernible appearance with the low transmission in the other direction.[29,30] Therefore, exploiting anisotropic metallic nanoapertures with polarization-switchable coloration for optical encryption could better avoid confusion in eye recognition.

Hiding information provides another degree of freedom to strengthen the security level. The aforementioned approaches of concealed images based on chemical stimuli-responsive characteristics usually require sophisticated installation and facilities, imposing great difficulties to potential counterfeiters, but also hindering the practical deployment of the security tag. A universally compatible platform, which can adapt to diversified architectures, is hence highly desirable. Polymer-dispersed liquid crystals (PDLCs), a composite material system with micrometer-scale liquid crystal (LC) droplets randomly dispersed inside a polymer host, demonstrate a milky opaque appearance.[31–33] Driven by an external voltage, the LC director will re-orientate, satisfying an index-matching condition between the LCs and the polymer host. As a result, PDLCs become completely transparent. In addition to electric driving, some other driving schemes including optical, magnetic, and acoustic fields[34–37] have been also developed. The premixture solution of PDLCs has controllable mobility, facilitating its conformal coverage on nanostructures with arbitrarily complex geometries. Furthermore, flexible substrates can be used,

owing to the high mechanical elasticity of the polymer matrix after photopolymerization.[38–43] These advantageous features make PDLCs excellent candidates for steganographic optical encryption. However, to the best of our knowledge, no attempt to exploit PDLCs for optical cryptography and image encryption applications has been reported.

In this work, we propose an electrically switchable, polarization-sensitive optical encryption scheme based on PDLC-integrated aluminum nanoaperture arrays. An anisotropic nanoaperture provides the polarization-dependent plasmonic resonances, producing a clear color when the incident polarization is aligned along the nanoaperture's short axis, and a diminished pale color with the incident polarization aligned along its long axis. In contrast, a square nanoaperture creates indistinguishable plasmonic resonances for both polarizations. With proper arrangement of the asymmetric and symmetric nanoapertures, multiplexed information encryption can be independently generated via only changing the illumination polarization. The addition of PDLCs further enables the hided information to be electrically readable. To validate the concept, we experimentally demonstrate the dual images with embedded profiles and polarization-sensitive quick response (QR) codes encoded with an arbitrary pixel size and further confirm the encryption performance of the information. Experimental results suggest that PDLC-integrated aluminum nanoaperture arrays could be used for many applications including high-security optical encryption, security tags, anti-counterfeiting, multichannel imaging, and dynamic displays.

While asymmetric nanoaperture arrays intrinsically exhibit a strong polarization-sensitive intensity contrast, which arises from the coupling of surface plasmon polaritons (SPPs)[29,30,44] symmetric ones have no polarization dependence. Given the intensity degeneracy in one polarization direction for rectangular and square nanoapertures, one can create polarization-

sensitive images by arranging rectangular and square nanoapertures in a designed manner. This lays the foundation of polarization-dependent information display by manipulating the incident polarization. Fig. 1a and 1b show the schematic designs of two nanoaperture arrays in an aluminum film. The first one is an array of rectangular nanoapertures, with a width of 110 nm and a length of 220 nm, square-arranged with a lattice pitch of 390 nm. The other one is a square array with the nanoaperture width of 260 nm, square-arranged with a larger lattice pitch of 470 nm. The rectangular nanoaperture was purposely designed to only respond for incident visible light with polarization aligned along its short axis. In this work, the incident polarization angle is set to be θ

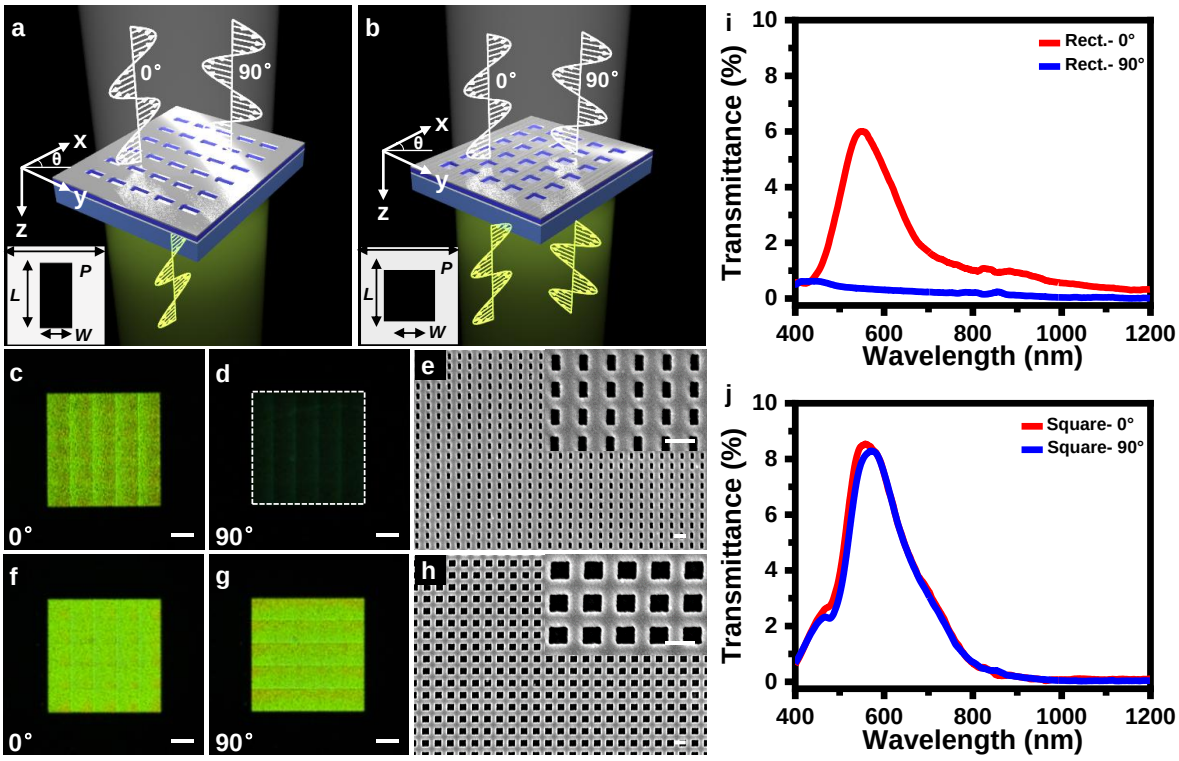

Figure 1. Schematic illustration of the plasmonic resonances of rectangular (a) and square (b) nanoaperture arrays under the incident light with $\theta = 0°$and $\theta = 90°$. (c, d, e) and (f, g, h) Optical ($\theta = 0°$and $\theta = 90°$) and SEM images of the rectangular ($W =$ 110 nm, $L = 220$ nm, $P = 390$ nm) and square ($W = L = 260$ nm, $P = 470$ nm) nanoaperture arrays. Scale bars are 20 μm in optical

images and 400 nm in SEM images. (i, j) Corresponding optical transmission spectra for the incident light with θ = 0°and θ = 90°.

with respect to the *x*-axis in Fig. 1a and 1b. By changing the dimensions and periodicities, we have achieved the polarization-dependent and polarization-independent plasmonic colors in the whole visible range based on rectangular (Fig. S1a and S1c) and square (Fig. S1b and S1d) nanoapertures. The parameters of the nanoapertures are set as the following: the length to width ratio of rectangular nanoaperture is fixed to be 2/1 and the square nanoaperture has the same size as the length of the rectangular nanoaperture. The length increases from 100 to 420 nm with a step size of 40 nm from bottom to top. The lattice pitch varies from 210 to 530 nm with a step size of 20 nm from left to right. In the following, we only take the green color marked in Fig. S1 with a green solid line box as an example to demonstrate our proposed concept. Upon incidence, the rectangular nanoaperture array whose short axis is parallel to the *x*-axis shows a yellowish-green and dim appearance at θ = 0°and θ = 90°, respectively, as shown in Fig. 1c and 1d. In contrast, the square nanoaperture array demonstrates the almost same yellowish-green appearance for both θ = 0°and θ = 90° cases, as shown in Fig. 1f and 1g. More importantly, both rectangular and square nanoaperture arrays respond similarly to *x*-polarized illumination. The scanning electron microscopy (SEM) morphologies of rectangular (Fig. 1e) and square (Fig. 1h) nanoaperture arrays demonstrate the sharp edges and uniform surface morphologies, indicating high-quality fabrication. The experimentally measured actual size is about 15 nm larger than the designed value, ascribing to the nanofabrication errors. Fig. 1i and 1j show the measured transmission spectra that correspond to the nanoaperture arrays in Fig. 1e and 1h, respectively. The spectra reveal that the rectangular nanoaperture array has distinctive polarization-sensitive transmittance with $T_{\theta=0^\circ} \approx$ 6% and $T_{\theta=90^\circ} \approx 0$, while the square nanoaperture array has nearly

the same transmittance with $T_{\theta = 0°} \approx T_{\theta = 90°} \approx 8.5\%$, showing a polarization-insensitive nature. The low transmittance originates from the nanoaperture nature. However, the elimination of the lift-off will greatly simplify the whole nanofabrication processes. Moreover, there is still room to further improve the transmission efficiency. For example, adding one layer of refractive index matching materials or arranging the lattice hexagonally to increase the lattice symmetry are effective approaches to further improve the transmittance.[45,46] In addition, the nanoapertures themselves are diffraction-limited and the array periods also approach the diffraction limit. Therefore, the diffraction effect of the propose nanoaperture arrays can be neglected. In this work, we mainly consider the case of normal incidence. Under the oblique incidence, the plasmonic resonance will be blue-shifted due to the increase of the in-plane wave vector of incident light.[47]

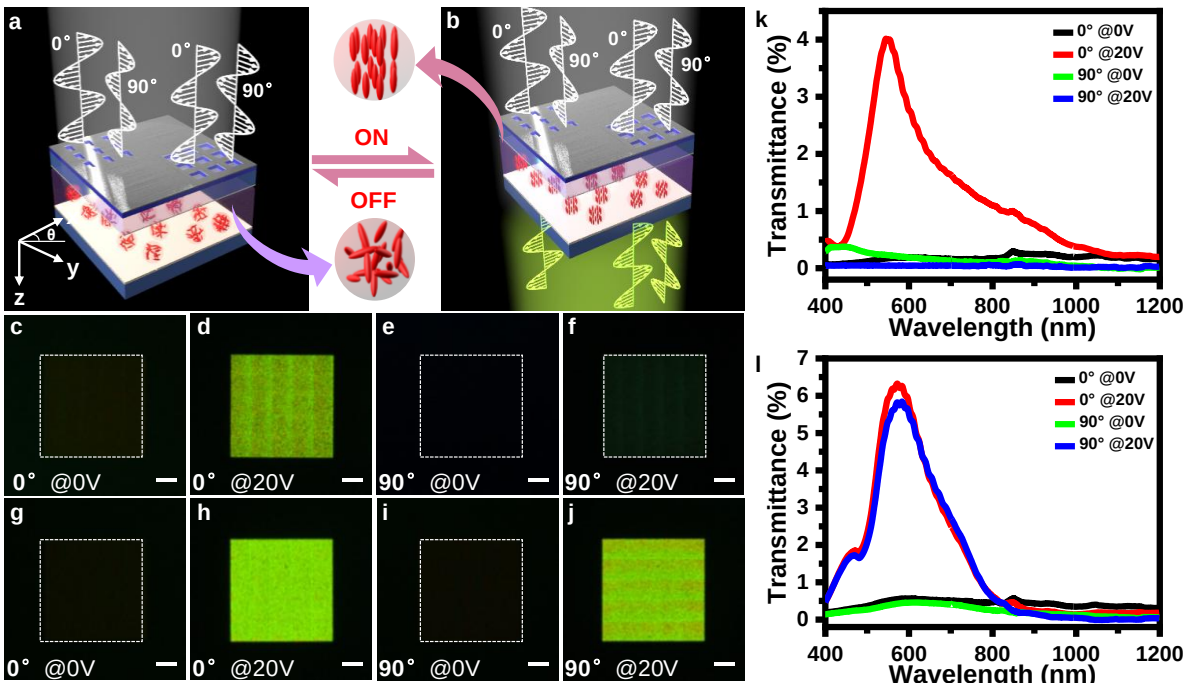

Figure 2. Schematic diagram of electrically switchable transmission based on PDLC-integrated nanoapertures arrays at "OFF" (a) and "ON" (b) states, respectively. Optical images under the illumination with $\theta = 0°$and $\theta = 90°$ at $V = 0$ V (c, e and g, i) and

V = 20 V (d, f and h, j) for the rectangular (c–f) and square (g–j) nanoaperture arrays. Scale bar: 20 μm. (k, l) Measured optical transmission spectra for the rectangular (k) and square (l) nanoaperture arrays with θ = 0°and θ = 90° at V = 0 V and V = 20 V, respectively.

Overlaying a PDLC layer onto the other side of the substrate with the nanoaperture arrays makes it possible to electrically switch the arrays' transmission, hence providing another degree of information encryption. Fig. 2a and 2b show the schematic of switchable transmission based on PDLC-integrated nanoaperture arrays before and after applying an external electric field. Inside the PDLC film, there are plenty of microscale LC droplets formed during the photopolymerization-induced phase separation process upon UV exposure.[32,33] The fabricated PDLC film has a typical morphology with the LC droplet size of ~2.18 μm in diameter, as shown in Fig. S2. In the "OFF" state, the LC droplets have a different refractive index from the polymer host, causing strong scattering of the incident light and subsequently illustrating an opaque state regardless of the incident polarization. When applying a sufficient voltage on the PDLC film, the LC director will be re-aligned along the electric field direction, satisfying the index-matching condition between the LCs and the polymer host. Consequently, the PDLC film becomes totally transparent and the composite systems show similar optical behaviors as the bare nanoaperture arrays. Without applying the voltage, the composite systems have a completely dark appearance with no transmission for all cases, as shown in Fig. 2c, 2e, 2g, and 2i. Upon applying a voltage of 20 V, Fig. 2d and 2f presents the polarization-sensitive color appearance for the rectangular nanoaperture array. While Fig. 2h and 2j illustrate the polarization-insensitive appearance for the square nanoaperture array. Fig. 2k and 2l show the measured optical transmission spectra of the composite systems when V = 0 V and V = 20 V, further confirming the observed results in Fig. 2c–2j. We can see that the addition of the PDLC layer can completely switch the transmission of the nanoaperture arrays, resulting in a high switching contrast. Nothing that besides PDLCs,

other types of LC-based techniques,[48–51] such as holographic PDLCs and cholesteric LCs, can be also integrated with metasurfaces to extend the functions or improve the performance.

From Figs. 1 and 2, we can see that both rectangular and square nanoaperture arrays demonstrate a quite similar color appearance at θ = 0° regardless of the PDLC layer. This provides a useful degeneracy for information encryption. Therefore, we can encrypt information by elaborately arranging the rectangular and square nanoapertures. As an example, we have designed a symbol

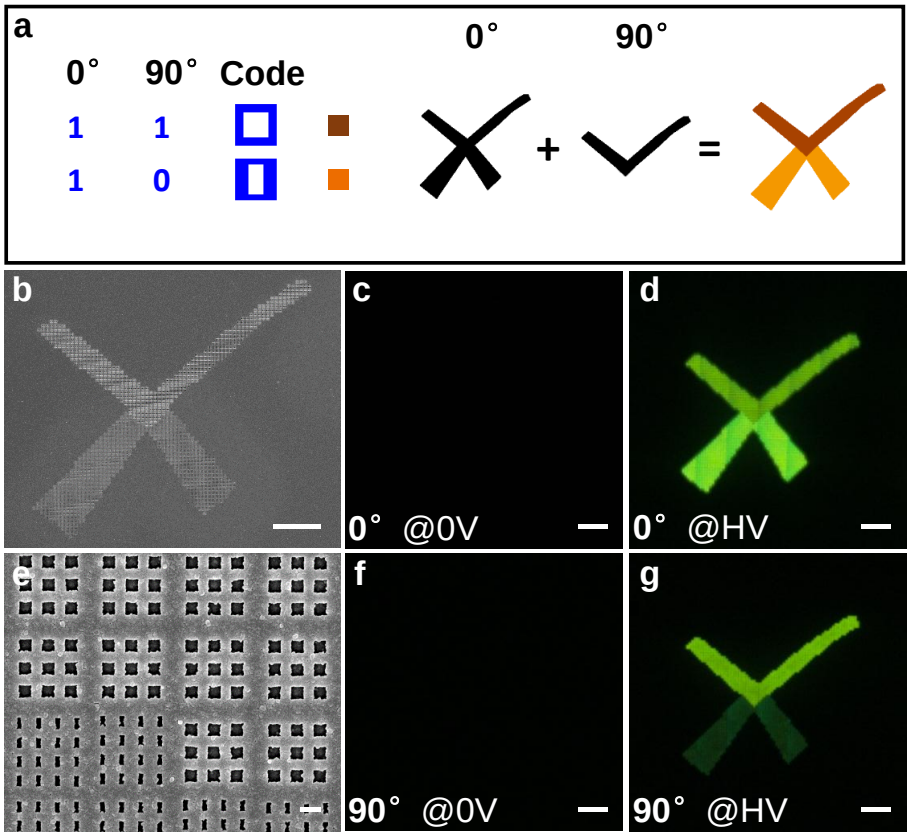

Figure 3. An experimental demonstration of the electrically switchable, polarization-sensitive information encryption. (a) Illustrative diagram of our encoding scheme. (b, e) Typical SEM images of the whole and partially magnified encrypted patterns. Electrically switchable, polarization-sensitive images at θ = 0° (c, d), θ = 90° (f, g), V = 0 V (c, f), and V = 20 V (d, g), respectively. Scale bar: 20 μm in b–d, f, g; 400 nm in e.

"×" including the symbol "✓" inside it. The encoding scheme is shown in Fig. 3a. The symbol "✓" is presented with the square nanoaperture arrays, while the rest of the "×" is filled with the rectangular nanoaperture arrays with the nanoaperture's short-axis parallel to the *x*-axis. Fig. 3b and 3e show the typical SEM morphologies of our sample with arranged rectangular and square nanoaperture arrays. The encrypted symbol was experimentally demonstrated in Fig. S3 in the supporting information. When the incident polarization angle $\theta = 0°$, a clear, yellowish-green "×" logo appears. By changing the polarization angle to $\theta = 90°$, the symbol "✓" is clearly distinguishable. With the inclusion of the PDLC layer, Fig. 3c and 3d demonstrate the switching effect of the "×" at $\theta = 0°$. As expected, we can hardly see the embedded "✓" with the applied voltage. In contrast, at $\theta = 90°$, a fully dark image and a bright "✓" symbol can be clearly seen in Fig. 3f and 3g, respectively. It is worth mentioning that in Fig. 3g, a dim "×" profile is still visually recognizable due to nonnegligible transmission along the long-axis of the rectangular nanoaperture. The cell thickness and exposure intensity dominate the dark appearance at the "OFF" state.[52] Here, we overlaid one PDLC layer with its thickness of 45 μm that was exposed to a UV intensity of 40 mW/cm^2.

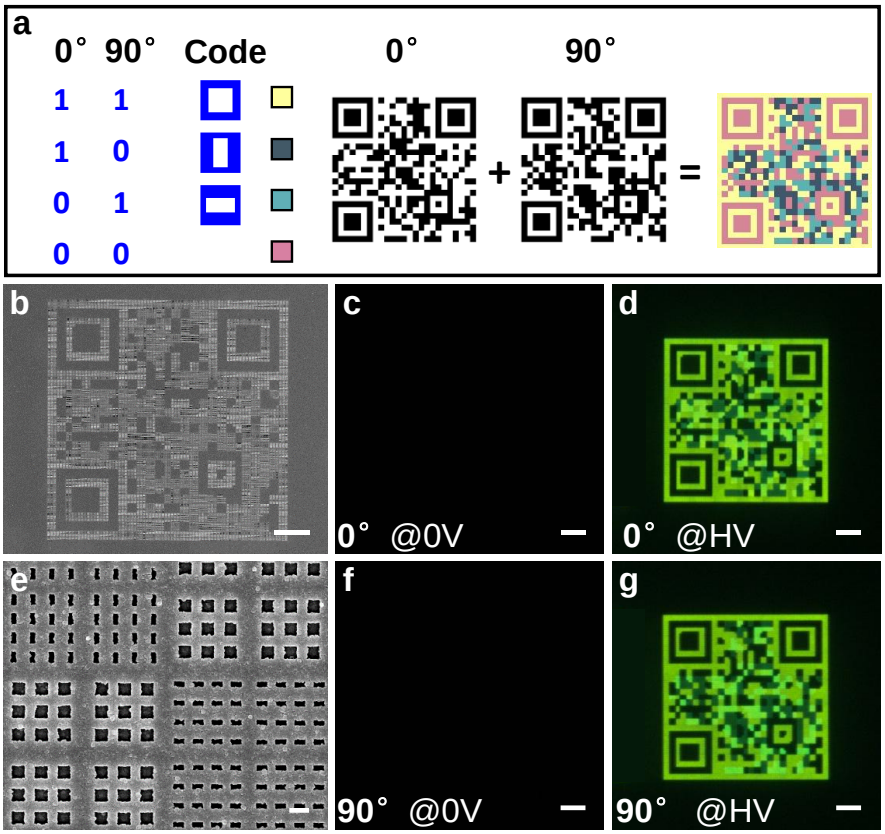

Figure 4. An experimental demonstration of the electrically switchable, polarization-controlled dual-channel information encryption. (a) Schematic of the coding scheme for polarization-dependent QR design. (b, e) SEM images of the whole QR and locally magnified patterns. Electrically switchable, polarization-sensitive QR images at θ = 0° (c, d), θ = 90° (f, g) at V = 0 V (c, f), and V = 20 V (d, g), respectively. Scale bar: 20 μm in b–d, f, g; 400 nm in e.

As known, the binary coding scheme (i.e., two representing symbols of 0 and 1) is widely used for information expression and interchange. In analogy to the binary coding scheme, we can therefore make use of the polarization-sensitive transmission characteristics for cryptography applications. As a proof-of-concept, Fig. 4 demonstrates a QR code image with two polarization-encoded messages. Fig. 4a shows the designed coding scheme by exploiting the combination of rectangular and square nanoapertures. A square nanoaperture forms the coding unit with the same resonance in two crossed polarization directions. A rectangular nanoaperture is the coding unit that responds only to the incident polarization aligned along its short axis. Other responses

are coded with no aperture, i.e. an opaque layer of aluminum that blocks the light so that the sample appears dark regardless of the incident polarization. Consequently, we can encode a pixel with four states representing by “1 1”, “1 0”, “0 1”, and “0 0” instead of the only complementary states of “0 1” and “1 0”.17 We encoded the word “NANOSTRUCTURE” into the QR1 that responds to the polarization at $\theta = 0°$, and the word “LIQUID CRYSTALS” into the QR2 with responses to the polarization at $\theta = 90°$. The fabricated sample exhibited the polarization-recognizable QR images, as shown in Fig. S3a and S3b. Upon the 0°-polarized incidence, the square nanoapertures will exhibit yellowish-green color, and the rectangular nanoapertures with the short axis parallel to the x-axis will also have a similar appearance. Both cases are identified as the bright pixels in the QRs. While other pixels are designated as dark ones. We can observe the same bright and dark distribution as the designed QRs. Therefore, we can reliably identify the coded information by scanning these QRs. Fig. 4b and 4e show the SEM images of the fabricated sample representing the whole pattern and locally magnified patterns. Again, by adding the PDLC layer on the other side of the substrate with the nanoapertures, we can hide the QRs at the OFF state of the PDLCs, as shown in Fig. 4c and 4f, hence providing one more degree to enhance the information security. At the ON state of the PDLCs, the bright QR codes at $\theta = 0°$ and $\theta = 90°$ are two independent messages that are scannable, as shown in Fig. 4d and 4g. By rotating the polarization angles to 45° and 135°, the QR images became unreadable, as shown in Fig. S4c and S4d, indicating a high-security level of the QRs. We have also successfully demonstrated the polarization-dependent QRs with the other colors, as shown in Fig. S5. To verify the superiority of our proposed QR encryption, we simultaneously coded two encrypted QRs with the same information in the 90° incidence but different messages in the

crossed direction, as shown in Fig. S6. These experimental results prove that our encrypted QR principle can work with high reliability and flexibility.

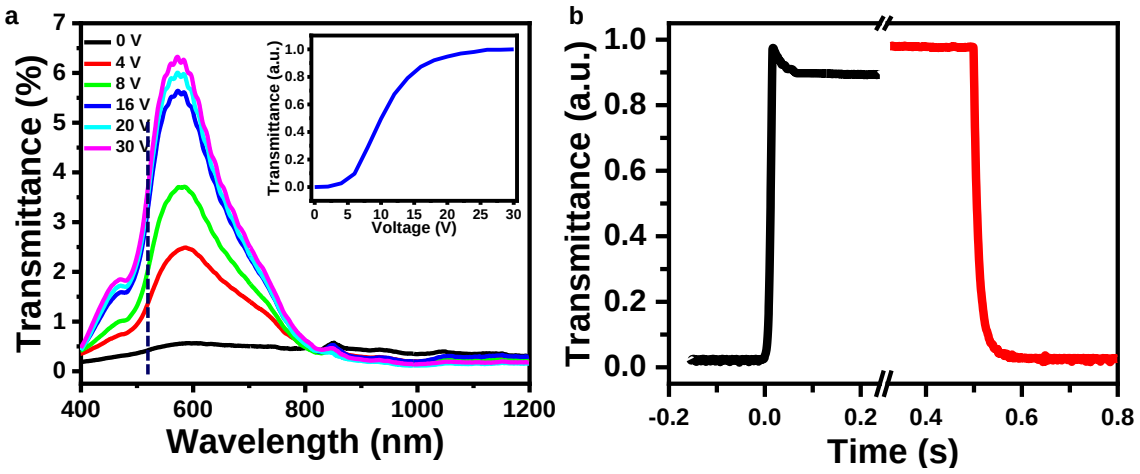

Figure 5. (a) The changes of transmission spectra with the applied voltage of the PDLC-integrated square nanoaperture arrays. Inset shows the transmittance changes with the applied voltage at the selected wavelength of 520 nm marked with a dash line in (a). (b) The retrieved rising (black line) and falling (red line) times at the switching voltage of 17 V.

Switching speed (or response time) is also a key parameter to evaluate an electrically switchable device. The response time is the sum of both rising and falling times. The rising time is mainly governed by the applied voltage and cell thickness. While the falling time is mainly determined by the droplet size.[52] We further measured the response time of the PDLC-integrated aluminum nanoaperture arrays with the LC droplet size of ~2.18 μm in diameter. Fig. 5a shows the changes of optical transmission at different applied voltages for the PDLC-integrated square nanoaperture arrays. By fixing the wavelength at 520 nm, we can then track the transmittance changes versus the applied voltage, as shown in the inset in Fig. 5a. The switching voltage corresponding to the 90% normalized transmission is 17 V. The rising and falling times in Fig. 5b are 8.7 and 29.8 ms, respectively. Generally, higher exposure intensity will induce a faster polymerization rate and subsequently smaller LC droplet size. In another sample with the PDLC

thickness of 45 μm that was exposed to the UV source at 40 mW/cm^2 for 10 min, the LC droplets have an averaged size ~1.24 μm in diameter. We have achieved a shorter falling process (~16.3 ms) but a longer rising time (~68.2 ms), as shown in Fig. S7. Therefore, there should be a compromise between the rising and falling times so that the total response time can be further reduced. Overall, the PDLC-integrated nanoaperture arrays demonstrate a quite fast switching speed compared to other chemical reaction-based information encryption schemes that usually have a response time of seconds.[21,25]

In summary, we have proposed and experimentally validated an electrically switchable, polarization-sensitive optical encryption scheme using PDLC-integrated aluminum nanoaperture arrays. Asymmetric and symmetric nanoapertures respectively exhibit polarization-sensitive and polarization-insensitive plasmonic resonance characteristics. This enables the encryption of optical images via a designed arrangement of asymmetric and symmetric nanoapertures. An additional degree of information encryption is achieved with the integration of the PDLCs, hiding the message regardless of the incident polarization. We have demonstrated high-quality encrypted images and QRs with electrically switchable, polarization-sensitive properties based on PDLC-integrated aluminum nanoaperture arrays. The switching speed can reach 38 ms at 17 V. The current metasurface nanoaperture arrays still suffer from many drawbacks such as long and expensive nanofabrication. However, with the advances of the nanofabrication techniques, these issues could be further solved to a great extent. Our proposed technique regarding the PDLC-integrated aluminum nanoapertures could be applied to many fields including easy-to-read security tags, anti-counterfeiting, multichannel imaging, and dynamic displays.

METHODS

PDLC-integrated nanoaperture arrays fabrication: The PMMA 4.5% (ARP672.045, 950k 4.5 wt% in anisole, Germany) was spin-coated on the non-conductive side of the indium-tin-oxide (ITO) glass substrate at 5000 rpm/s with an acceleration of 500 rpm/s^2 for 1 min. The PMMA layer has a thickness of ~260 nm. Then another layer of conductive adhesive was spin-coated onto the PMMA layer at 1500 rpm/s with the acceleration of 500 rpm/s^2 for 1 min to make the substrate conductive. Then electron-beam lithography (EBL) (Nanobeam-nB5, England) was carried out at 80 kV with the writing dose of 700 μC/cm^2. After that, the development process was carried out. The substrate was firstly flushed with deionized water for 30 s to remove the conductive adhesion. Then it was developed in the solution mixture containing 25% MIBK and 75% IPA in volume for 55 s. After development, the sample was rinsed in IPA solution for 30 s and then blown with nitrogen. To remove the residual PMMA, ICP (GSE200Plus, North Microelectronics Company, China) treatment was carried out for 10 s with the O_2 plasma. After that, the thickness of the PMMA profile is about 200 nm. A 50 nm-thick aluminum layer was deposited by the DC magnetron sputtering (KYKY-500CK-500ZF, KYKY Technology Co., Ltd., China). The nanoaperture arrays were finally fabricated. Another cleaned ITO glass substrate was adhered to the ITO surface of the nanoaperture sample to form a cell with a controlled gap. The prepolymer mixture of NOA 65 (Norland Products, Inc., America) and LC E7 (Jiangsu Hecheng Display Co., Ltd., China) with their mass ratio of 3:7 was infiltrated into the LC cell through the capillary action. The refractive index of NOA 65 is 1.52. The ordinary and extraordinary refractive indices of E7 are n_o = 1.52 and n_e = 1.74 at room temperature, respectively. The cell with a thickness of 10 μm in Fig. 2 and 5 was exposed to the UV source (UVEC-4 Ⅰ Ⅰ Ⅰ, LOTS, China) at 20 mW/cm^2 for 10 min. The cell with a thickness

of 45 μm in Fig. 3 and 4 was exposed to the same source at 40 mW/cm^2 for 10 min. Finally, the PDLC-integrated aluminum nanoaperture arrays were achieved.

Characterization: The investigation of surface morphologies of nanoapertures were carried out using the field-emission scanning electron microscopy (FESEM) (GeminiSEM 300-71-10, Zeiss, Germany) with a voltage of 5 kV at in-lens mode. The optical images of the nanoaperture arrays under the incident polarization angle of θ = 0° and θ = 90° were taken by a polarized optical microscope (Nikon 'pi', Japan), which was equipped with a 20 W Halogen source and rotatable polarizer at 20× objective lens with NA = 0.3. The PDLC-integrated aluminum nanoaperture arrays were driven by a square-wave voltage with a frequency of 1 kHz from a signal generator (ATA-2041, Aigtek, China). The optical transmission spectra of samples were collected using a UV-Vis-NIR microspectrophotometer (20/30 PVTM, CRAIC Technologies, America) equipped with a 75 W xenon light source and a linear polarizer. The response times were measured through a homemade setup including a helium-neon laser operating at 532 nm (REO 33361, Research Electro-Optics Co., Ltd., America), collimating lens, detector (Model 2031, Newport, America), and oscilloscope (DPO2024, Tektronix, USA).

ASSOCIATED CONTENT

Supporting Information

The Supporting Information is available free of charge at http://pubs.acs.org.

Polarization-dependent and polarization-independent plasmonic colors based on rectangular and square nanoaperture arrays covering the whole visible range, SEM images and LC droplet size distribution of PDLCs fabricated at the UV exposure intensity of 20 mW/cm^2, encrypted symbols and QRs based on the bare aluminum nanoapertures; polarization-dependent QRs for the blue

and orange colors, experimental demonstration of two polarization-dependent QRs with the same information at the 90°-polarized incidence and different information at 0°-polarized incidence, and SEM morphologies, LC droplet size distribution, transmission spectra, and response time of PDLCs fabricated at the UV exposure intensity of 40 mW/cm^2.

AUTHOR INFORMATION

Corresponding Author

Davy Gérard – *Light, nanomaterials, nanotechnologies (L2n), Université de Technologie de Troyes & CNRS ERL 7004, 10004 Troyes, France;* Email: davy.gerard@utt.fr

Yan Jun Liu – *Department of Electrical and Electronic Engineering, Southern University of Science and Technology, Shenzhen 518055, China; Key Laboratory of Energy Conversion and Storage Technologies (Southern University of Science and Technology), Ministry of Education, Shenzhen 518055, China; State Key Laboratory of Applied Optics, Changchun Institute of Optics, Fine Mechanics and Physics, Chinese Academy of Sciences, Changchun 130033, China;* Email: yjliu@sustech.edu.cn

Author

Ke Li – *Department of Electrical and Electronic Engineering, Southern University of Science and Technology, Shenzhen 518055, China; Light, nanomaterials, nanotechnologies (L2n), Université de Technologie de Troyes & CNRS ERL 7004, 10004 Troyes, France；*

Jiawei Wang − *Department of Electrical and Electronic Engineering, Southern University of Science and Technology, Shenzhen 518055, China；*

Wenfeng Cai − *Department of Electrical and Electronic Engineering, Southern University of Science and Technology, Shenzhen 518055, China；*

Huilin He − *Department of Electrical and Electronic Engineering, Southern University of Science and Technology, Shenzhen 518055, China; Harbin Institute of Technology, Harbin 150001, China;*

Mengjia Cen − *Department of Electrical and Electronic Engineering, Southern University of Science and Technology, Shenzhen 518055, China;*

Jianxun Liu − *Department of Electrical and Electronic Engineering, Southern University of Science and Technology, Shenzhen 518055, China;*

Dan Luo − *Department of Electrical and Electronic Engineering, Southern University of Science and Technology, Shenzhen 518055, China;*

Quanquan Mu − *State Key Laboratory of Applied Optics, Changchun Institute of Optics, Fine Mechanics and Physics, Chinese Academy of Sciences, Changchun 130033, China;*

Notes

The authors declare no competing financial interest.

ACKNOWLEDGMENT

This work was supported in part by National Natural Science Foundation of China (Grant No. 62075093), China Postdoctoral Science Foundation (2020M672697), Guangdong Innovative and Entrepreneurial Research Team Program (Grant No. 2017ZT07C071), Natural Science Foundation of Guangdong Province (Grant No. 2019A1515110864), Shenzhen Science and Technology Innovation Commission (Grant No. JCYJ20180305180635082, GJHZ20180928155207206, and JCYJ20170817111349280), and Open Fund of State Key Laboratory of Applied Optics (Grant No. SKLAO-201904). The authors also acknowledge the assistance of SUSTech Core Research Facilities.

ABBREVIATIONS

PDLC, polymer-dispersed liquid crystal; SPPs, surface plasmon polaritons; UV, ultraviolet; ITO, indium tin oxide; QR, quick response; EBL, electron-beam lithography; FESEM, field-emission scanning electron microscopy; NA, numerical aperture.

REFERENCES

1 Zang, X.; Dong, F.; Yue, F.; Zhang, C.; Xu, L.; Song, Z.; Chen, M.; Chen, P. Y.; Buller, G. S.; Zhu, Y.; Zhuang, S.; Chu, W.; Zhang, S.; Chen, X. Polarization Encoded Color Image Embedded in a Dielectric Metasurface. *Adv. Mater.* **2018**, 30, 1707499.

2 Li, J.; Kamin, S.; Zheng, G.; Neubrech, F.; Zhang, S.; Liu, N. Addressable Metasurfaces for Dynamic Holography and Optical Information Encryption. *Sci. Adv.* **2018**, 4, eaar6768.

3 Song, M.; Wang, D.; Kudyshev, Z. A.; Xuan, Y.; Wang, Z.; Boltasseva, A.; Shalaev V. M.; Kildishev A. V. Enabling Optical Steganography, Data Storage, and Encryption with Plasmonic Colors. *Laser Photon. Rev.* **2021**, 15, 2000343.

4 Yu, N.; Genevet, P.; Kats, M. A.; Aieta, F.; Tetienne, J.-P.; Capasso, F.; Gaburro, Z. Light Propagation with Phase Discontinuities: Generalized Laws of Reflection and Refraction. *Science* **2011**, 334, 333–337.

5 Kuznetsov, A. I.; Miroshnichenko, A. E.; Brongersma, M. L.; Kivshar, Y. S.; Luk'yanchuk, B. Optically Resonant Dielectric Nanostructures. *Science* **2016**, 354, 6314.

6 Sun, S.; He, Q.; Xiao, S.; Xu, Q.; Li, X.; Zhou, L. Gradient-Index Meta-Surfaces as a Bridge Linking Propagating Waves and Surface Waves. *Nat. Mater.* **2012**, 11, 426–431.

7 Arbabi, A.; Horie, Y.; Bagheri, M.; Faraon, A. Dielectric Metasurfaces for Complete Control of Phase and Polarization with Subwavelength Spatial Resolution and High Transmission. *Nat. Nanotechnol.* **2015**, 10, 937–943.

8 Kumar, K.; Duan, H.; Hegde, R. S.; Koh, S. C. W.; Wei, J. N.; Yang, J. K. W. Printing Colour at the Optical Diffraction Limit. *Nat. Nanotechnol.* **2012**, 7, 557–561.

9 Kristensen, A.; Yang, J. K. W.; Bozhevolnyi, S. I.; Link, S.; Nordlander, P.; Halas, N. J.; Mortensen, N. A. Plasmonic Colour Generation. *Nat. Rev. Mater.* **2016**, 2, 16088.

10 Heydari, E.; Sperling, J. R.; Neale, S. L.; Clark, A. W. Plasmonic Color Filters as Dual-State Nanopixels for High-Density Microimage Encoding. *Adv. Funct. Mater.* **2017**, 27, 1701866.

11 Yang, W.; Xiao, S.; Song, Q.; Liu, Y.; Wu, Y.; Wang, S.; Yu, J.; Han, J.; Tsai, D.-P. All-dielectric metasurface for high-performance structural color. *Nat. Commun.* **2020**, 11, 1864.

12 Duempelmann, L.; Luu-Dinh, A.; Gallinet, B.; Novotny, L. Four-Fold Color Filter Based on Plasmonic Phase Retarder. *ACS Photon.* **2016**, 3, 190–196.

13 Li, Z.; Clark, A. W.; Cooper, J. M. Dual Color Plasmonic Pixels Create a Polarization Controlled Nano Color Palette. *ACS Nano* **2016**, 10, 492–498.

14 Chen, Y.; Yang, X.; Gao, J. 3D Janus Plasmonic Helical Nanoapertures for Polarization-Encrypted Data Storage. *Light Sci. Appl.* **2019**, 8, 45.

15 Goh, X. M.; Zheng, Y.; Tan, S. J.; Zhang, L.; Kumar, K.; Qiu, C. W.; Yang, J. K. W. Three-Dimensional Plasmonic Stereoscopic Prints in Full Colour. *Nat. Commun.* **2014**, 5, 5361.

16 Jang, J.; Jeong, H.; Hu, G.; Qiu, C. W.; Nam, K. T.; Rho, J. Kerker-Conditioned Dynamic Cryptographic Nanoprints. *Adv. Opt. Mater.* **2019**, 7, 1801070.

17 Jung, C.; Yang, Y.; Jang, J.; Badloe, T.; Lee, T.; Mun, J.; Moon, S. W.; Rho, J. Near-Zero Reflection of All-Dielectric Structural Coloration Enabling Polarization-Sensitive Optical Encryption with Enhanced Switchability. *Nanophotonics* **2020**, 10, 919–926.

18 Deng, J.; Deng, L.; Guan, Z.; Tao, J.; Li, G.; Li, Z.; Li, Z.; Yu, S.; Zheng, G. Multiplexed Anticounterfeiting Meta-Image Displays with Single-Sized Nanostructures. *Nano Lett.* **2020**, 20, 1830–1838.

19 Cai, J.; Zhang, C.; Li, W. Di. Dual-Color Flexible Metasurfaces with Polarization-Tunable Plasmons in Gold Nanorod Arrays. *Adv. Opt. Mater.* **2020**, 2001401, 1–8.

20 Kim, T.; Yu, E.-S.; Bae, Y.-G.; Lee, J.; Kim, I. S.; Chung, S.; Lee, S.-Y.; Ryu, Y.-S. Asymmetric Optical Camouflage: Tuneable Reflective Colour Accompanied by the Optical Janus Effect. *Light Sci. Appl.* **2020**, 9, 175.

21 Duan, X.; Liu, N. Scanning Plasmonic Color Display. *ACS Nano* **2018**, 12, 8817–8823.

22 Zhang, C.; Jing, J.; Wu, Y.; Fan, Y.; Yang, W.; Wang, S.; Song, Q.; Xiao, S. Stretchable All-Dielectric Metasurfaces with Polarization-Insensitive and Full-Spectrum Response. *ACS Nano* **2020**, 14, 1418-1426.

23 He, J.; Zhang, M; Shu, S.; Yan, Y.; Wang, M. VO_2 Based Dynamic Tunable Absorber and Its Application in Switchable Control and Real-Time Color Display in the Visible Region. *Opt. Express* **2020**, 28, 37590–37599.

24 Sharma, M.; Hendler, N.; Ellenbogen, T. Electrically Switchable Color Tags Based on Active Liquid-Crystal Plasmonic Metasurface Platform. *Adv. Opt. Mater.* **2020**, 8, 1901182.

25 Lee, G.; Kong, M.; Park, D.; Park, J.; Jeong, U. Electro-Photoluminescence Color Change for Deformable Visual Encryption. *Adv. Mater.* **2020**, 32, 1907477.

26 Franklin, D.; He, Z.; Ortega, P. M.; Safaei, A.; Cencillo-Abad, P.; Wu, S.-T.; Chanda, D. Self-Assembled Plasmonics for Angle-Independent Structural Color Displays with Actively Addressed Black States. *Proc. Natl. Acad. Sci. U. S. A.* **2020**, 117, 13350–13358.

27 Liu, Y.; Lee, Y. H.; Zhang, Q.; Cui, Y.; Ling, X. Y. Plasmonic nanopillar arrays encoded with multiplex molecular information for anticounterfeiting applications. *J. Mater. Chem. C* **2016**, 4, 4312–4319.

28 Liu, Y.; Lee, Y. H.; Lee, M. R.; Yang, Y.; Ling, X. Y. Flexible Three-Dimensional Anticounterfeiting Plasmonic Security Labels: Utilizing Z-Axis-Dependent SERS Readouts to Encode Multilayered Molecular Information. *ACS Photon.* **2017**, 4, 2529–2536.

29 Koerkamp, K. J. K.; Enoch, S.; Segerink, F. B.; Van Hulst, N. F.; Kuipers, L. Strong Influence of Hole Shape on Extraordinary Transmission through Periodic Arrays of Subwavelength Holes. *Phys. Rev. Lett.* **2004**, 92, 183901.

30 Gordon, R.; Brolo, A. G.; McKinnon, A.; Rajora, A.; Leathem, B.; Kavanagh, K. L. Strong Polarization in the Optical Transmission through Elliptical Nanohole Arrays. *Phys. Rev. Lett.* **2004**, 92, 037401.

31 Liu, Y. J.; Sun, X. W. Electrically Switchable Computer-Generated Hologram Recorded in Polymer-Dispersed Liquid Crystals. *Appl. Phys. Lett.* **2007**, 90, 191118.

32 Liu, Y. J.; Sun, X. W. Holographic Polymer-Dispersed Liquid Crystals: Materials, Formation, and Applications. *Adv. Optoelectron.* **2008**, 684349.

33 Li, K.; Jiang, H.; Cheng, M.; Li, Y.; Yin, Z.; Luo, D.; Sun, X. W.; Liu, Y. J. Controlling Morphological and Electro-Optical Properties via the Phase Separation in Polymer/Liquid-Crystal Composite Materials. *Liq. Cryst.* **2020**, 47, 238–247.

34 Guo, S. M.; Liang, X.; Zhang, C. H.; Chen, M.; Shen, C.; Zhang, L. Y.; Yuan, X.; He, B. F.; Yang, H. Preparation of a Thermally Light-Transmittance-Controllable Film from a Coexistent System of Polymer-Dispersed and Polymer-Stabilized Liquid Crystals. *ACS Appl. Mater. Interfaces* **2017**, 9, 2942–2947.

35 Liu, Y. J.; Ding, X.; Lin, S. C. S.; Shi, J.; Chiang, I. K.; Huang, T. J. Surface Acoustic Wave Driven Light Shutters Using Polymer-Dispersed Liquid Crystals. *Adv. Mater.* **2011**, 23, 1656–1659.

36 de Sio, L.; Lloyd, P. F.; Tabiryan, N. V.; Bunning, T. J. Hidden Gratings in Holographic Liquid Crystal Polymer-Dispersed Liquid Crystal Films. *ACS Appl. Mater. Interfaces* **2018**, 10, 13107–13112.

37 Zhang, C.; Guo, Z.; Zheng, X.; Zhao, X.; Wang, H.; Liang, F.; Guan, S.; Wang, Y.; Zhao, Y.; Chen, A.; Zhu, G.; Wang, Z. L. A Contact-Sliding-Triboelectrification-Driven Dynamic Optical Transmittance Modulator for Self-Powered Information Covering and Selective Visualization. *Adv. Mater.* **2020**, 32, 1904988.

38 Murray, J.; Ma, D.; Munday, J. N. Electrically Controllable Light Trapping for Self-Powered Switchable Solar Windows. *ACS Photon.* **2017**, 4, 1–7.

39 Cong, S.; Cao, Y.; Fang, X.; Wang, Y.; Liu, Q.; Gui, H.; Shen, C.; Cao, X.; Kim, E. S.; Zhou, C. Carbon Nanotube Macroelectronics for Active Matrix Polymer-Dispersed Liquid Crystal Displays. *ACS Nano* **2016**, 10, 10068–10074.

40 Cheng, Z.; Wang, T.; Li, X.; Zhang, Y.; Yu, H. NIR-Vis-UV Light-Responsive Actuator Films of Polymer-Dispersed Liquid Crystal/Graphene Oxide Nanocomposites. *ACS Appl. Mater. Interfaces* **2015**, 7, 27494–27501.

41 Chiou, C. C.; Hsu, F. H.; Petrov, S.; Marinova, V.; Dikov, H.; Vitanov, P.; Dimitrov, D.; Hsu, K. Y.; Lin, Y. H.; Lin, S. H. Flexible Light Valves Using Polymer-Dispersed Liquid Crystals and TiO_2/Ag/TiO_2 Multilayers. *Opt. Express* **2019**, 27, 16911.

42 Khlifi, S.; Bigeon, J.; Amela-Cortes, M.; Dumait, N.; Loas, G.; Cordier, S.; Molard, Y. Switchable Two-Dimensional Waveguiding Abilities of Luminescent Hybrid Nanocomposites for Active Solar Concentrators. *ACS Appl. Mater. Interfaces* **2020**, 12,

14400–14407.

43 Nasir, N.; Hong, H.; Rehman, M. A.; Kumar, S.; Seo, Y. Polymer-Dispersed Liquid-Crystal-Based Switchable Glazing Fabricated: Via Vacuum Glass Coupling. *RSC Adv.* **2020**, 10, 32225–32231.

44 van der Molen, K. L.; Klein Koerkamp, K. J.; Enoch, S.; Segerink, F. B.; van Hulst, N. F.; Kuipers, L. Role of Shape and Localized Resonances in Extraordinary Transmission through Periodic Arrays of Subwavelength Holes: Experiment and Theory. *Phys. Rev. B* **2005**, 72, 045421.

45 Im, H.; Lindquist, N. C.; Lesuffleur, A.; Oh, S.-H. Atomic Layer Deposition of Dielectric Overlayers for Enhancing the Optical Properties and Chemical Stability of Plasmonic Nanoholes. *ACS Nano* **2010**, *4*, 947–954.

46 Wang, Q.-J.; Li, J.-Q.; Huang, C.-P.; Zhang, C.; Zhu, Y.-Y. Enhanced Optical Transmission through Metal Films with Rotation-Symmetrical Hole Arrays. *Appl. Phys. Lett.* **2005**, *87*, 091105.

47 Genet, C.; Ebbesen, T. W. Light in Tiny Holes. *Nature* **2007**, *445*, 39–46.

48 Xiong, J.; Yin, K.; Li, K.; Wu, S.-T. Holographic Optical Elements for Augmented Reality: Principles, Present Status, and Future Perspectives. *Adv. Photon. Res.* **2021**, *2*, 2000049.

49 Chen, P.; Ma, L.-L.; Duan, W.; Chen, J.; Ge, S.-J.; Zhu, Z.-H.; Tang, M.-J.; Xu, R.; Gao, W.; Li, T.; Hu, W.; Lu, Y.-Q. Digitalizing Self-Assembled Chiral Superstructures for Optical Vortex Processing. *Adv. Mater.* **2018**, *30*, 1705865.

50 De Sio, L.; Roberts, D. E.; Liao, Z.; Hwang, J.; Tabiryan, N.; Steeves, D. M.; Kimball, B. R. Beam Shaping Diffractive Wave Plates. *Appl. Opt.* **2018**, *57*, A118–A121.

51 Chen, P.; Ma, L.-L.; Hu, W.; Shen, Z.-X.; Bisoyi, H. K.; Wu, S.-B.; Ge, S.-J.; Li, Q.; Lu, Y.-Q. Chirality Invertible Superstructure Mediated Active Planar Optics. *Nat. Commun.* **2019**, *10*, 2518.

52 Drzaic, P. S. Droplet Density, Droplet Size, and Wavelength Effects in PDLC Light Scattering. *Mol. Cryst. Liq. Cryst.* **1995**, *261*, 383–392.

ToC